Desorption of the C_2^- Anion from the Au−C-Deposited Y_2O_3-Stabilized ZrO_2 Surface

Quanxin Li,*,† Masateru Nishioka,† Hodeo Kashiwagi,† Yoshifumi Torimoto,‡ and Masayoshi Sadakata*,†

Department of Chemical System Engineering, School of Engineering, The University of Tokyo, 7-3-1 Hongo, Bunkyo-ku, Tokyo 113-8656, Japan, and Production Technology Institute of Kao Corporation, 1334 Minato, Wakayama 640, Japan

Received: January 16, 2002; In Final Form: July 31, 2002

Carbon dimer anions (C_2^-) and atomic oxygen radical anions (O^-) desorbed from an Au−C-deposited Y_2O_3-stabilized ZrO_2 (YSZ) surface have been observed. Both the emitted anions and electrons were found to be strongly dependent on the surface temperature and applied extraction field. The Arrhenius plots for the anions and electrons exhibit double-linear behavior, resulting in lower apparent activation energies in the high-temperature region (>913 K). It was found that the apparent activation energies can be reduced by the extraction field. Measurements of the absolute emission current density show similar temperature and field features as derived by TOF (time-of-flight) spectroscopic investigations. The observed anions of O^- are attributed to the detachment of the transient anions of $O^{2-}(s)$ (i.e., $O^{2-}(s) \rightarrow O^-(s) + e^-(s)$), which migrate from the YSZ bulk onto the emission surface. The $C_2^-(s)$ anions are attributed to the surface anion-exchange reactions between $O^-(s)$ and surface carbon atoms. An emission mechanism is proposed to account for the observed temperature dependence, field characteristics, and emission branch ratios of the desorbed anions and electrons.

1. Introduction

The chemistry of radical anions is an important and interesting field both for fundamental and applied science, as indicated by numerous studies of reactions involving these species in the gas phase and in the condensed phase.[1,2] Recently, the studies of anions have been pushed mainly by various needs such as electrochemically promoted catalytic reactions,[3−9] surface modification of materials,[10−12] biochemical materials,[2,13−15] and the ion chemistry of the earth's atmosphere.[16−19] Particularly, a new and attractive catalytic effect, named as nonfaradaic electrochemical modification of catalytic activity (NEMCA effect) of metals interfaced with solid electrolytes, has been demonstrated to alter the catalytic reaction rate in a very pronounced, controllable, and reversible way by the pioneering work of Vagenas et al.[3,5−9] The modification of the catalytic activity of the metal film is attributed to spill-over ionic species, which migrate from the solid electrolyte onto the metal surface and cause a work function change of the metal surface.

It is well-known that the Y_2O_3-stabilized ZrO_2 (YSZ) electrolyte, possessing significant ionic conductivity for the transient anion of O^{2-}, has been widely used for electrochemical promotion catalyst reactions, fuel cells, and oxygen sensors.[3,7−9,20−25] When the anions of O^{2-} are supplied to a metal-catalyst film deposited on YSZ and exposed to $C_2H_4-O_2$ or $CO-O_2$ mixtures, it causes a dramatic increase of the catalytic oxidation rate, which reaches 10^2-10^5 times higher than the supply rate of O^{2-} to the catalyst.[6] This indicates that each O^{2-} supplied to the catalyst will cause 10^2-10^5 absorbed O atoms to react with C_2H_4 or CO and form CO_2 and H_2O. More recently, the mechanism for the electrochemical modification of catalytic activity has been further clarified by the investigations of temperature-programmed desorption of oxygen from Pt films deposited on the YSZ surface.[5] It was also confirmed that the anions of O^{2-} were not formed via adsorption from the gas phase. The bond energy of absorbed oxygen decreases with an increasing catalyst potential and work function.

To develop a simple and economic method to generate ionic radicals, we have proposed a new approach by using a solid electrolyte as an ionic radical emitter.[26,27] This approach is expected to obtain high purity and sustainable ionic radicals in the gas phase because a solid electrolyte may be possessed of good ionic conductivity only for special ions (like an ion filter), and the continuous ion implantation into the electrolyte can be simply realized by supplying electron and oxygen opposite to the emission surface (e.g., the electrocatalytic reaction of $O_2(g)$ to O^{2-}: $^1/_2O_2 + 2e^- \rightarrow O^{2-}$). The transient anion of O^{2-} is very unstable, and a rapid dissociation will occur as it migrates from the electrolyte bulk into the emission surface. The sustainable O^- emission, indeed, has been observed from the Au- or Ag-deposited Y_2O_3-stabilized ZrO_2 (YSZ) electrolyte.[26,27] However, the quantitative emission features and desorption mechanism remain to be revealed.

In this report, we present the investigations of anions and electrons desorbed from the Au−C-deposited YSZ surfaces by our new developed time-of-flight (TOF) system. The motivation of this study was not only to provide a new approach for generating the carbon-containing negative ions, which are the key chemical species for the diamondlike carbon film preparation,[11,39,40] but also to obtain a clearer mechanistic picture for the formation, reaction, and desorption of anionic radicals from the solid electrolyte surface.

2. Experimental Section

A commercially used tubular YSZ specimen (Nikato Corp.) with an outer diameter of 17 mm, a thickness of 3 mm, and a length of 600 mm was used in this experiment. As indicated in

* Corresponding authors. E-mail: sadakata@chemsys.t.u-tokyo.ac.jp and liqx@chemsys.t.u-tokyo.ac.jp.
† The University of Tokyo.
‡ Production Technology Institute of Kao Corporation.

10.1021/jp020114s CCC: $25.00
Published on Web 10/22/2003

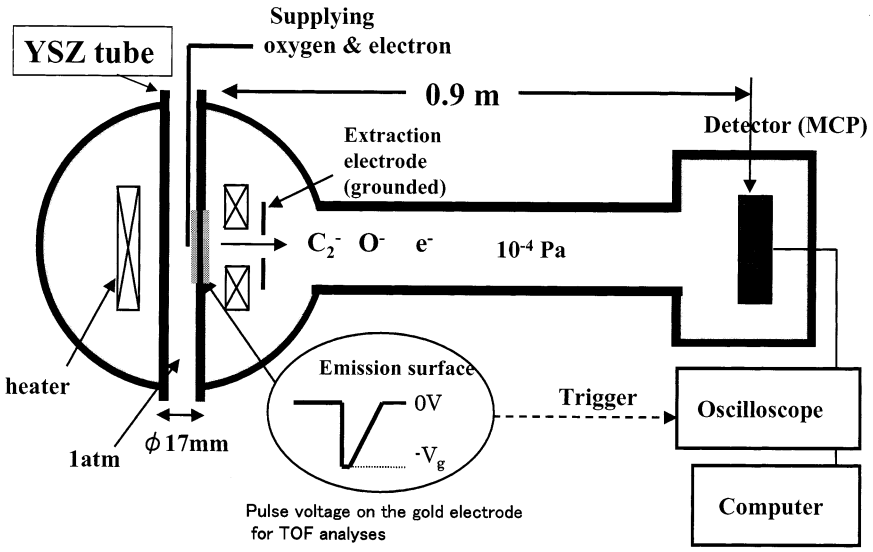

Figure 1. Schematic diagram of the experimental apparatus, which mainly consists of two sections: a sampling chamber and an ion-detection chamber equipped with a TOF mass spectrometer for measuring the desorbed anions and electrons from the Au- or Au−C-deposited YSZ electrolyte surface.

Figure 1, a thin and uniform Au film was deposited on the outside surface of the YSZ specimen with a length of 30 mm. The inside wall of the tubular YSZ was also coated by the Au paste to supply electrons. Then the specimen was dried at 500 °C for 1 h and calcinated to 800 °C with a heating rate of 15 °C/min. To eliminate impurities on the Au-deposited emission surface, the specimen was treated at 800 °C for 8 h under flowing dried oxygen. To prepare the Au−C film, activated carbon powder with a diameter of ∼200 μm (Wako Chemical Co.) was uniformly mixed with Au paste (Nilaco Co.). The weight ratio between activated carbon and Au in the mixture was about 1.7%. Then, a thin and uniform Au−C layer was covered on the outside surface of the YSZ specimen with a length of 30 mm by the Au−C mixture. The coated YSZ specimen was dried at 400 °C for 1 h and calcinated at 650 °C under flowing dried oxygen for 8 h. The weight of the Au−C layer formed on the YSZ surface ranged from 2.5 to 4.5 mg/cm^2.

The experimental apparatus is divided into two sections: a sampling chamber and an ion-detection chamber equipped with the usual time-of-flight (TOF) mass spectrometer (Figure 1), which are pumped by two turbo molecular pumps. The deposited YSZ specimen was mounted in the center of the sampling chamber. The emission surface of the YSZ tube (in the vacuum) was opposite to the ion detector and heated radiatively by an Fe−Cr alloy filament. The heater was quartz-sealed in order to avoid the possible influence of electron emission from it. The surface temperature was measured by a Ni/NiCr thermocouple. To continuously implant O^{2-} into the YSZ electrolyte, we supplied electrons and oxygen to the inside surface of the YSZ tube, where O^{2-} can be generated by the electrocatalytic reaction of O_2 to O^{2-} (i.e., $^1/_2O_2 + 2e^- \rightarrow O^{2-}$).[6] The formed O^{2-} then migrates through the YSZ solid electrolyte onto the emission surface (in the vacuum) by field-enhanced thermal diffusion. The anions and electrons desorbed from the surface were extracted by an extraction electrode, which is mounted opposite to the emission surface with a changeable distance from 1 to 5 cm. The extraction field strength was determined by the applied potential on the emission surface and the distance between the emission surface and the extraction electrode. The anionic collection electrode was connected to a picoampermeter for total emission current measurements. In the center of the collection plate, there was a pinhole with a diameter of 0.2 mm, which allows simultaneous analysis by the TOF spectrometer.

The emitted anions and electrons were mass-analyzed by the TOF mass spectrometer. The TOF spectrometer was equipped with a variable flight tube (generally used length: 90 cm), mounted on two tandem microchannel plates (Chevron-type MCP, gain: $4 \times 10^6-1 \times 10^7$), which was operated in the negative-ion detection mode. The output signal of MCP was amplified by an amplifier, recorded by a digital oscilloscope, and finally acquired by a computer-controlled counter system. The collection efficiencies for ions and electrons emitted depend on the length of the flight tube, the MCP response efficiencies of the ionic species, the applied extraction field, and the size of the sampling pinhole. We estimated the collection efficiency by changing the length of the flight tube (0.7−2.1 m) and the diameter of the sampling pinhole (ϕ = 0.2−5 mm) at a given extraction.

3. Results and Discussion

3.1. Emission Features of Anions and Electrons. The anionic species emitted from the solid surface were mass-analyzed by TOF mass spectrometry. The TOF spectra consist of several broadened profiles in the present case (Figure 2), which may be due to wide speed and angular distributions of the emitted species. When the YSZ electrolyte surface was deposited by a thin and uniform gold (Au) layer, two peaks (profiles) were clearly observed in the mass range of 0−100, as shown in Figure 2. One peak, located at the far left, corresponds to the electrons emitted from the surface. Another has a mass number of 16, which corresponds to the O^- anions emitted. Alternately, as the YSZ surface was deposited by an Au−C mixture layer, a new peak appeared around mass number 24 in the TOF spectrum (Figure 2), which is attributed to the anions of C_2^-. In Figure 2b, two small profiles (peak positions: m/z = 36 and 44) were identified at 988 K, which were tentatively assigned to the C_3^- and CO_2^- anions desorbed from the Au−C-deposited surface. These weak profiles were not found for the Au-deposited YSZ surface. The assignments of mass spectra were carried out by calculations of flight times and were further confirmed by quadrupole mass spectrometry.

The relative emission intensities of C_2^-, O^-, and electrons are shown in Figure 3 as a function of temperature. Both the

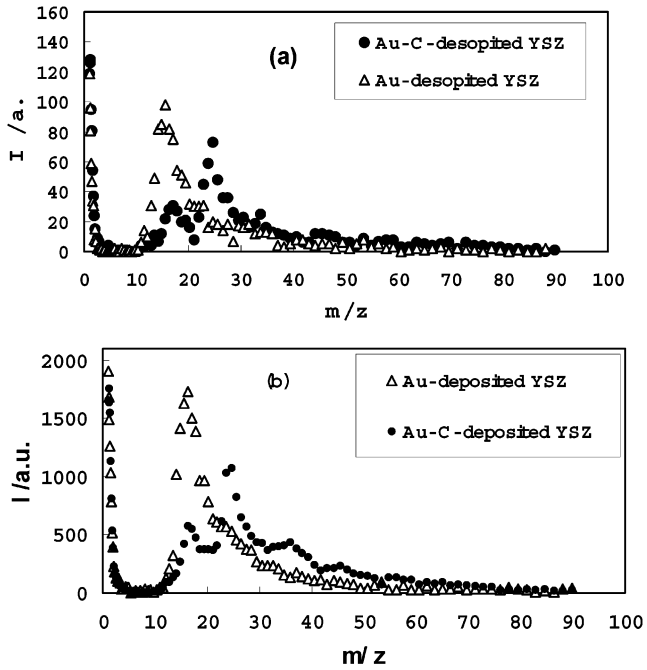

Figure 2. Typical TOF mass spectra of anions and electrons desorbed from the Au- and Au−C-deposited YSZ surfaces: (a) 853 K and 500 V/cm; (b) 988 K and 500 V/cm.

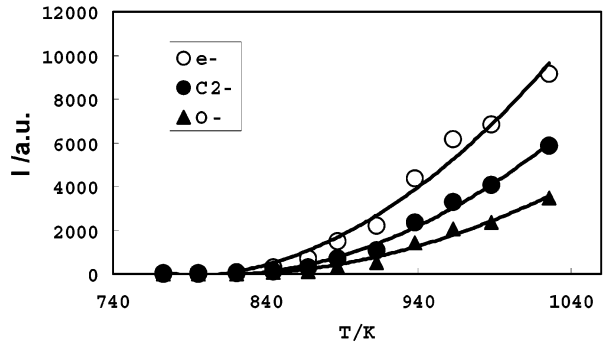

Figure 3. Temperature dependence of e^-, C_2^-, and O^- desorbed from the Au−C-deposited YSZ surface in a fixed extraction field of 500 V/cm.

emitted anions and electrons strongly depend on the surface temperature. The emission of anions and electrons is very weak below 773 K and significantly increases when the surface temperature is over 883 K. The emission intensities are also plotted versus temperature in Arrhenius fashion, ln I versus $1/T$, to derive the apparent activation energy from the relation $I = A \exp(-E_a/RT)$, where A, E_a, and R are the preexpotenial factor, the apparent activation energy, and the gas constant, respectively. Figure 4 shows a typical Arrhenius plot for the C_2^- emission from the Au−C-deposited YSZ surface at a field of 500 V/cm. Interestingly, the ln I versus $1/T$ curve cannot be described by a single straight line in the temperature region of 773−1023 K. Alternately, the plot is more suitably represented by two straight lines in the high- and low-temperature regions, respectively. Accordingly, two types of apparent activation energies, expressed by E_{LT} and E_{HT}, were derived from the ln I versus $1/T$ curves in the low-temperature region (<913 K) and the high-temperature region (>913 K) respectively, which are summarized in Table 1.

However, the emission intensities of the anions and electrons from the Au−C-deposited YSZ surface are sensitive to the applied extraction field. Figure 5 displays the relative emission intensities of C_2^-, O^-, and electrons against the extraction field

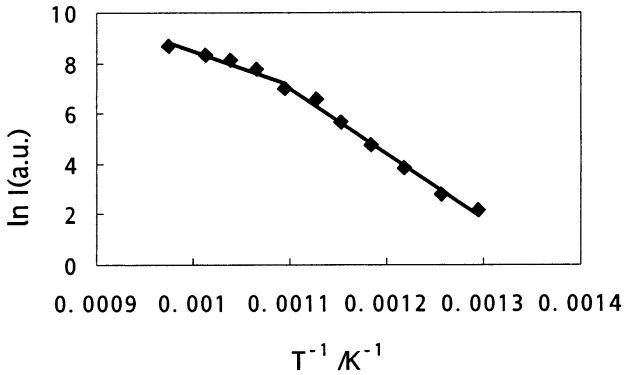

Figure 4. Arrhenius plot for desorbed C_2^- at 500 V/cm. It exhibits double-line behavior and has a larger apparent activation energy in the low-temperature region (<913 K).

TABLE 1: Activation Energies of C_2^-, O^-, and e^- Measured at Different Extraction Fields[a,b]

V/cm	$E_{LT}(C_2^-)$	$E_{HT}(C_2^-)$	$E_{LT}(O^-)$	$E_{HT}(O^-)$	$E_{LT}(e^-)$	$E_{HT}(e^-)$
200	265.3	92.6	282.2	97.5	236.7	92.8
300	274.1	95.7	248.3	128.8	233.4	127.6
400	251.3	91.1	244.1	106.7	200.7	94.9
500	212.4	80.7	220.3	116.2	203.0	63.9
600	210.9	55.7	246.4	91.4	204.5	74.0
700	201.0	48.1	202.6	71.5	193.4	58.9
800	206.7	46.4	192.3	81.0	181.7	61.0

[a] E_{LT} and E_{HT} stand for the apparent activation energies measured in the low-temperature region (<913 K) and the high-temperature region (>913 K), respectively. [b] The unit of the activation energy is kJ/mol.

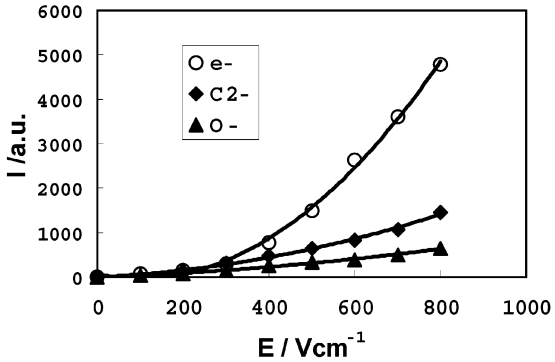

Figure 5. Relative emission intensities of e^-, C_2^-, and O^- desorbed from the Au−C-deposited YSZ surface were measured as a function of the extraction field at 887 K.

at a fixed temperature of 887 K. When the extraction field (E) is less than 200 V/cm, the emission intensity of the C_2^- anion is very weak. No measurable emission was observed at $E = 0$ within our experimental detection limitation. As the field is over 200 V/cm, the C_2^- emission progressively increases as the extraction field increases. The emission threshold value of the field for the C_2^- emission (i.e., the extrapolation value of the $I-E$ curve to give the intercept with the x-axis) somewhat decreases as the surface temperature increases. It is worth noting that the observed field characteristics could not be attributed to the detection efficiency of the TOF system (distance effect) because the space emission current, even if it was detected at a close distance of 1 cm from the emission surface, also exhibited the same field effects (see Figure 8b).

Furthermore, it was found that the apparent activation energies for the anion emission can be decreased by the applied extraction field. Figure 6shows the field dependencies of the apparent activation energies for the C_2^- anion emission from the Au−C-deposited YSZ surface. The apparent activation energies,

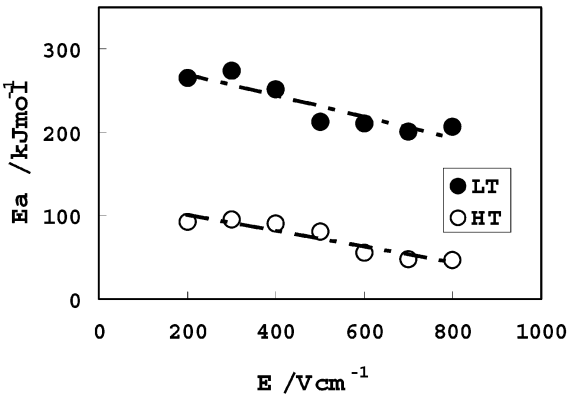

Figure 6. Apparent activation energies of C_2^- versus the extraction field, which were derived in the low-temperature (LT) region (<913 K) and the high-temperature (HT) region (>913 K).

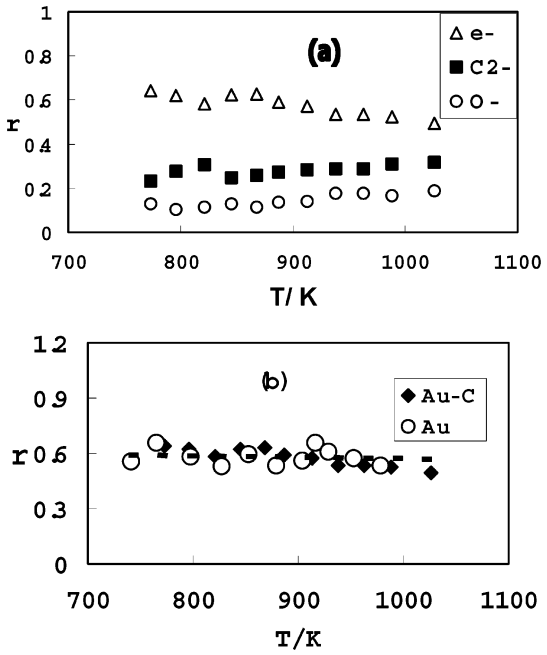

Figure 7. (a) Emission-branch ratios of e^-, C_2^-, and O^- (i.e., $r(C_2^-)$, $r(O^-)$, and r (e^-), respectively) as a function of surface temperature from the Au−C-deposited YSZ surface. (b) Comparison of the emission-branch ratios of electrons measured for the Au- and Au−C-deposited YSZ surfaces.

derived both from the high- and low-temperature regions, were reduced by the applied field. Similar features were also observed for the O^- and electron emissions, as shown in Table 1. These field-enhanced effects on the emission would be attributed to the reduction of the surface barrier height and to the increase of O^{2-}(s) coverage by the external field, which will be discussed in detail in section 3.4.

The emission branch ratio of the anion, $r(X^-)$, is defined as the relative intensity ratio of emitted anions of X^- to total anions and electrons. Similarly, the emission-branch ratio of electrons, $r(e^-)$, is teamed with the relative intensity ratio of electrons to total anions and electrons. Figure 7a shows the emission-branch ratios for C_2^-, O^-, and electrons (i.e., $r(C_2^-)$, $r(O^-)$, and $r(e^-)$, respectively) as a function of surface temperature. The emission-branch ratio of electrons varies in the range of 0.5−0.6, which is larger than the ratios of C_2^- and O^-. The emission of C_2^- from the Au−C-deposited YSZ surface is about two times stronger than that of O^-. In addition, the emission-branch ratios of C_2^- and O^- appear to increase gradually with increasing temperature in our investigated region. The emission-branch ratio

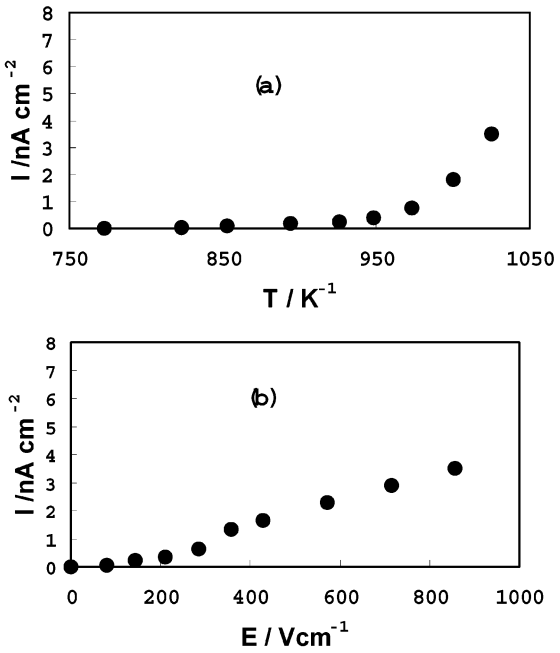

Figure 8. (a) Absolute emission current density versus surface temperature at an extraction field of 1000 V/cm. (b) Absolute emission current density versus extraction field at 1023 K.

of electrons, by contrast, drops from 0.6 to 0.5 when the temperature rises from 773 to 1023 K. It was also shown that the emission-branch ratios of electrons, both from the Au- and the Au−C-deposited YSZ surfaces, were nearly identical, as shown in Figure 7b. This observation may indicate that the emitted C_2^- anions would not originate from the electron-attachment reactions occurring on the Au−C-deposited YSZ surface.

The absolute emission current density has been measured simultaneously by a picoampermeter. Typical current−temperature ($I-T$) and current−field ($I-E$) characteristics are shown in Figure 8. The emission current density is also strongly sensitive to the surface temperature as well as the extraction field. The emission current is weak (on the order of 10 pA/cm^2) when temperature is below 873 K, and thereafter a significant increase occurs in the region 873−1023 K (Figure 8a). However, the measured current density progressively increases at fields above 200 V/cm (Figure 8b). The maximum emission current density of 3.5 nA/cm^2 was obtained at 1023 K and 1000 V/cm in our investigated region.

3.2. Electron and O^- Emission. The electron emission observed in this study might not be the field electron emission, which only likely occurs when a large electron field is applied to a metal tip or a plate.[29−31] The field electron emission, described by the famous Fowler−Nordheim equation,[28] $I = aE^2 \exp(-b/E)$, has been realized from metals and semiconductors to various synthesized materials. Theoretically, no measurable emission would occur from a surface at field less than $\sim 10^7$ V/cm. Our applied field ($<10^3$ V/cm) would, in general, be too low to cause a field electron emission.

However, when a metal or an oxide filament is heated in a vacuum, electrons can also boil off its surface to form thermal electron emissions. Because the electrons require the least amount of thermal energy to overcome their binding energy in the solid, the thermal electron emission generally occurs at high temperature or from a metal surface with a low work function. Most importantly, thermal electron emission generally follows the well-known Richardson−Dushman (R−D) equation:[31]

$$I(e^-) = AT^2 \exp(-\phi/RT) \quad (1)$$

where $A = 4\pi emkb^2/h^3$ is a constant for a given metal surface and ϕ and R are the surface work function and the gas constant, respectively. For the electrons desorbed both from the Au- and Au−C-deposited YSZ surface, we found that the temperature behavior could not be described by the R−D theory. Hence, the electrons observed here might not be attributed to thermal electron emission.

It is well-known that the Y_2O_3-stabilized ZrO_2 (YSZ) solid electrolyte is a typical ionic conductor for O^{2-}.[3,7−9,20−25] Although the anions of O^{2-} can form and conduct in the bulk of YSZ, there is no evidence that O^{2-} exists in the gas phase according to our investigations. This implies that the transient anions of O^{2-} are very unstable on the electrode surface. A rapid detachment will occur when an anion transfers from the YSZ bulk to the electrolyte surface. Hence, this leads us to suggest the following mechanism to account for the observed electron and O^- emission from the Au- or Au−C-deposited YSZ surface.

The anions of O^{2-} can be formed initially by an electrochemical reduction reaction (i.e., $^1/_2O_2 + 2e^- \rightarrow O^{2-}$) by supplying oxygen and electrons to the inside surface of the YSZ tube.[5,6] Then the formed O^{2-} anions can be implanted into the YSZ electrolyte. After the O^{2-} anions migrate through the YSZ bulk into the emission surface by field-enhanced thermal diffusion, the rapid detachment of $O^{2-}(s)$ into $O^-(s)$ and $e^-(s)$ would occur on the surface. Finally, the dissociation products, $O^-(s)$ and electrons, can be desorbed into the gas phase. The above kinetic processes can be represented by

$$\begin{aligned} {}^1/_2O_2(g) + 2e^- &\rightarrow O^{2-}(is) \\ &\rightarrow O^{2-}(b) \rightarrow O^{2-}(s) \\ &\rightarrow O^-(s) + e^-(s) \\ &\rightarrow O^-(g)\uparrow + e^-(g)\uparrow \end{aligned} \tag{2}$$

where is, s, b, and g stand for the species on the inside surface of the YSZ tube, on the emission surface of YSZ (in the vacuum), in the bulk of YSZ, and in the gas phase, respectively. The above mechanism is also supported by the fact that the emission intensity of O^- is close to that of electrons from the Au-deposited YSZ surface because both desorbed O^- and electrons originate from the same detachment process of $O^{2-}(s)$.

We found that the emission intensity sharply decreased when the YSZ electrolyte was not deposited by the gold layer. This observation may indicate that the three-phase boundaries (TPB, i.e., the boundaries of the Au−YSZ gas phase) should play a very important role in the anionic emission processes. It has been found that the electrocatalytic reaction of the transformation of O^{2-} from the YSZ lattice to oxygen adsorbed on the metal-deposited film (i.e., $O^{2-} \rightarrow O + 2e^-$) takes place primarily at the three-phase boundaries.[8,33−35] In the present case, the detachment of O^{2-} into O^- and an electron may also occur at the three-phase boundary. Additionally, we believed that only a few electrons emit from the Au sites because of the large work function of Au (5.1 eV).[32] Hence, most of the electrons are expected to be emitted from the three-phase boundaries. However, there are two candidates for the desorption sites of O^- (i.e., the three-phase boundary (TPB) and the spot of Au). In the former, the O^- emission is likely rate-limited by a one-step process (i.e., $O^{2-}(TPB) \rightarrow O^-(TPB)\uparrow + e^-(TPB)\uparrow$). This is in contradiction to the experimental result, which shows that the O^- emission is correlated with two-step series processes in the high-temperature region (>913 K) and the low-temperature region (<913 K), respectively (see section 3.4). Thus, O^- may first migrate from the three-phase boundary to the Au surface and then be desorbed from the Au sites, which can be expressed by the following two-step process:

$$O^{2-}(TPB) \rightarrow O^-(TPB) \rightarrow O^-(\text{Au sites})\uparrow \tag{3}$$

In summary, the observed O^- and electrons can be attributed to the detachment of the intermediate anions of $O^{2-}(s)$ occurring on the emission surface. The electrons and the anions of $O^-(s)$ most likely desorb from the three-phase boundaries and the Au sites, respectively.

3.3. C_2^- Anion Emission. When the surface was deposited with an Au−C layer, the anion emission of C_2^-, whose intensity was about 2−3 times stronger than that of the O^- emission, was observed. To identify whether the emitted C_2^- anions originate from the possible ion reactions in the gas phase, we have investigated the O_2 pressure dependence of the anion emission. The results show that the intensities of O^- and C_2^- are nearly independent of O_2 pressure when it is lower than 1×10^{-6} Torr. Therefore, the observed C_2^- anions would predominantly originate from surface processes under the present background vacuum of $\sim 0.7 \times 10^{-4}$ Pa.

To account for the observed C_2^-, the following possible surface-chemistry modelings have been considered. In the first model, the formation of C_2^- starts from an electron attachment to the surface carbon atom C(s) to form $C^-(s)$, followed by the surface reaction of $C^-(s)$ and C(s) into $C_2^-(s)$ and desorption into the gas phase, which is represented by

$$e^-(s) + C(s) \rightarrow C^-(s) \tag{4}$$

$$C^-(s) + C(s) \rightarrow C_2^-(s) \tag{5}$$

$$C_2^-(s) \rightarrow C_2^-(g)\uparrow \tag{6}$$

This electron-attachment mechanism indicates that the C_2^- emission will in-situ reduce the electron emission intensity because part of the electrons are consumed by reaction 4. This prediction, however, is in contradiction to the experimental observations: (i) The emission-branch ratios of electrons both from the Au- and Au−C-deposited YSZ surface are approximately identical. (ii) The electron emission intensity is nearly independent of surface carbon (see Figures 2 and 7b).

The second candidate is the surface reaction between the transient anions of $O^{2-}(s)$ and carbon atoms, which is described by the following processes:

$$O^{2-}(s) + C(s) \rightarrow O^-(s) + C^-(s) \tag{7}$$

$$C^-(s) + C(s) \rightarrow C_2^-(s) \tag{8}$$

$$C_2^-(s) \rightarrow C_2^-(g)\uparrow \tag{9}$$

Also, the above mechanism appears to be unimportant for the observed C_2^- emission because it results in a simultaneous reduction of the electron emission by the consumption of O^{2-}. The C_2^- emission most likely originates from the charge-exchange reaction between $O^-(s)$ and C(s), which is expressed by

$$O^{2-}(s) \rightarrow O^-(s) + e^-(s) \tag{10}$$

$$O^-(s) + C(s) \rightarrow O(s) + C^-(s) \tag{11}$$

$$C^-(s) + C(s) \rightarrow C_2^-(s) \tag{12}$$

$$C_2^-(s) \rightarrow C_2^-(g)\uparrow \tag{13}$$

This mechanism indicates that the formation of C_2^- will cause a reduction of the O^- emission but not of the electron emission, which agrees with the experimental observations (Figure 2). Moreover, as temperature increased up to 650 °C, several weak profiles expected for the peaks of C_2^- and O^- were superimposed on the TOF spectra for the Au−C-deposited YSZ (Figure 2b). However, these profiles were not found in the TOF spectra for the Au-deposited YSZ surface. Thus, we suggested that other anionic products (e.g., C_3^- and CO_2^-), besides the C_2^- anions, were also formed by the surface reactions involving species such as C(s), C_2(s), C^-(s), C_2^-(s), O^-(s), and O_2^-(s). The quantitative measurements and analyses for these species were not carried out in the present study because of their weak intensities. However, no detectable peak of C^- was found in the TOF spectra. This is partly because the coverage of carbon on the surface is far greater than that of C^-(s) and partly because the surface reaction between C^-(s) and C(s) may be very fast if one notes that the electron affinities of C_2 and C are 3.5 and 1.27 eV respectively,[36] which leads to a very large exothermicity (855 kJ/mol) in the reaction. The emission intensity of C_3^- is considerably lower than that of C_2^- (Figure 2b), which would also be attributed to a lower electron affinity of C_3^- ($EA(C_3) = 2.0$ eV[41]) in comparison with that of C_2 ($EA(C_2) = 3.5$ eV[36]). Similarly, the expected emission intensity of C_3^- should be stronger than that of C^-, which is also in accord with the experimental observations.

3.4. Arrhenius Plots and Field Effects. On the basis of the aforementioned emission mechanism, the enhancement of anion emission with increasing temperature primarily causes (1) an increase of the O^{2-} diffusion in YSZ, which leads to an increase of the coverage of O^{2-}(s) on the emission surface and (2) an increases of the detachment rate of O^{2-}(s) into O^-(s) and of the desorption rate of O^-(s) from the surface at higher temperature. We also note that the measured Arrhenius plots ($\ln I - 1/T$ curves) for desorbed C_2^- exhibit double-linear behavior (see Figure 4). The apparent activation energies derived from the low-temperature region ($E_a = 207-265$ kJ/mol) are obviously larger than those from the high-temperature region ($E_a = 46-93$ kJ/mol). This phenomenon may indicate that the rate-controlling steps are different in the high-temperature region (>913 K) and low-temperature region (<913 K). The desorption activation energies of O^- and C_2^- from the Au surface have not been reported. We note that the apparent activation energy for the O^- emission in the low-temperature region (E_{LT}) varies in the range of 192−282 kJ/mol. The values are close to the binding energy of the oxygen atom on the Au surface (227−234 kJ/mol).[37,38] Thus, it seems that the O^- emission is controlled by the O^-(s) desorption from the Au spots in the low-temperature region. In the high-temperature region, the electron desorption to provide fresh three-phase boundaries or the electrochemical reaction to form O^{2-}(s) may determine the emission rate of O^-. Similarly, the C_2^- emission would be controlled by the C_2^-(s) desorption from the Au surface in the low-temperature region and by the electron desorption or the electrochemical reaction to form O^{2-}(s) in the high-temperature region.

According to the emission mechanism, the field characteristics of the anion and electron emissions can be explained as follows. First, because both the desorbed anions and electrons originate from the detachment of O^{2-}(s) on the surface, the emission rates of anions should depend on the coverage of O^{2-}(s) on the surface, which can be approximately expressed by the Elovich equation

$$\upsilon = \upsilon_0 \exp(-E_{desp}/RT) \exp(\beta\theta) \qquad (14)$$

where θ is the coverage of O^{2-}(s) on the surface, E_{desp} is the desorption activation energy of anions, and υ_0 and β are constants. The coverage of O^{2-}(s) on the surface is expected to increase with increasing field strength because the diffusion of O^{2-}(b) onto the emission surface is enhanced by the field. In addition, the extraction field reduces the surface barrier height because to leave the surface the anions must possess translational energy in excess of the potential, which binds it to the surface. According to the Arrhenius plots measured as a function of the field, the apparent activation energy indeed decreases with increasing field strength (Figure 6).

4. Conclusions

We report the formation and desorption of the carbon dimer anion (C_2^-) and atomic oxygen radical anion (O^-) from an Au−C-deposited Y_2O_3-stabilized ZrO_2 (YSZ) surface. The emission features of C_2^-, O^-, and electrons, including the temperature dependence, field characteristics, and emission-branch ratios, have been investigated. The O^- emission was attributed to the detachment of the transient anion of O^{2-}(s) occurring on the emission surface. The desorbed C_2^- anions were explained in terms of the surface anion-exchange reactions between O^-(s) and C(s). The anion emission may be controlled by desorption from the Au surface in the low-temperature region and by electron desorption to provide fresh three-phase boundaries or the electrochemical reaction to form O^{2-}(s) in the high-temperature region. The enhancement of anion emission by increasing temperature primarily causes (1) an increase of the O^{2-}(s) coverage on the emission surface, (2) an increase of the detachment rate of O^{2-}(s) into O^-(s) and e^-(s), and (3) an increase of the desorption rate of O^-(s) at higher temperature. The field effects on the anion and electron emission are attributed to changes in the O^{2-}(s) coverage and the surface barrier height by the external field. This contribution provides a new approach for generating the carbon-containing anions, which are the key chemical species in diamondlike carbon film preparation. We also showed direct experimental proof of the negative ionic surface reactions between O^- and C occurring on the metal/electrolyte catalyst surface.

Acknowledgment. This work was supported by core research for evolutional science and technology in JST (Japan Science and Technology). We are grateful to Professor Hosono, Dr. Yamanishi, and Dr. Hayashi for their motivating discussions on this work.

References and Notes

(1) Lee, J.; Grabowski, J. J. *Chem. Rev.* **1992**, *92*, 1611.
(2) Born, M.; Ingemann, S.; Nibbering, N. M. M. *Mass Spectrom. Rev.* **1997**, *16*, 181.
(3) Vayenas, C. G.; Tsiplakides, D. *Surf. Sci.* **2000**, *467*, 23.
(4) Poppe, J.; Volkening, S.; Schaak, A.; Schutz, E.; Janek, J.; Imbihl, R. *Phys. Chem. Chem. Phys.* **1999**, *1*, 5241.
(5) Neophytides, S. G.; Tsiplakides, D.; Vayenas, C. G. *J. Catal.* **1998**, *178*, 414.
(6) Vayenas, C. G.; Jaksic, M. M.; Bebelis, S. I.; Neophytides, S. G. In *Modern Aspects of Electrochemistry*; Bockris, J. O. M., Ed.; Plenum Press: New York, 1996; p 57.
(7) Vayenas, C. G.; Bebelis, S.; Ladas, S. *Nature (London)* **1990**, *343*, 625.
(8) Vayenas, C. G.; Ioannides, A.; Bebelis, S. *J. Catal.* **1991**, *129*, 67.
(9) Vayenas, C. G.; Bebelis, S.; Yentekakis, I., V.; Lintz, H. G. *Catal. Today* **1992**, *11*, 303.
(10) Ishikawa, J. *Rev. Sci. Instrum.* **1996**, *67*, 1410.
(11) Ishikawa, J. *Rev. Sci. Instrum.* **2000**, *71*, 1036.
(12) Tsuji, H.; Sato, H.; Baba, T.; Gotoh, Y.; Ishikawa, J. *Rev. Sci. Instrum.* **2000**, *71*, 797.

(13) Theruvathu, J. A.; Aravindakumar, C. T.; Flyunt, R.; von Sonntag, J.; von Sonntag, C. *J. Am. Chem. Soc*. **2001**, *123*, 9007.
(14) Flunt, R.; Schuchmann, M. N.; von Sonntag, C. *Chem.—Eur. J*. **2001**, *7*, 796.
(15) Santus, R.; Patterson, L. K.; Hug, G. L.; Bazin, M.; Maziere, J. C.; Morliere, P. *Free Radical Res*. **2000**, *33*, 383.
(16) Das, T. N. *J. Phys. Chem. A* **2001**, *105*, 9142.
(17) Neal, C.; Reynolds, B.; Adamson, J. K.; Stevens, P. A.; Neal, M.; Harrow, M.; Hill, S. *Hydrol. Earth Sys. Sci.* **1998**, *2/3*, 303.
(18) Viggiano, A. A.; Seeley, J. V.; Mundis, P. L.; Williamson, J. S.; Morris, R. A. *J. Phys. Chem. A* **1997**, *101*, 8275.
(19) Reiner, T.; Mohler, O.; Arnold, F. *J. Geophys. Res*. **1998**, *103*, 31309.
(20) Wang, D. Y.; Nowick, A. S. *J. Electrochem. Soc*. **1981**, *128*, 55.
(21) Zipprich, W.; Wiemhofer, H. D.; Vohrer, U.; Gopel, W. *Ber. Bunsen-Ges. Phys. Chem*. **1995**, *99*, 1406.
(22) Ladas, S.; Bebelis, S.; Vayenas, C. G. *Surf. Sci*. **1991**, *251/252*, 1062.
(23) Nicole, J.; Tsiplakides, D.; Wodiunig, S.; Comninellis, C. *J. Electrochem. Soc*. **1997**, *144*, 1312.
(24) Poppe, J.; Shaak, A.; Janek, J.; Imbihl, R. *Ber. Bunsen-Ges. Phys. Chem*. **1998**, *102*, 1019.
(25) Poppe, J.; Volkening, S.; Schaak, A.; Schutz, E.; Janek, J.; Imbihl, R. *Phys. Chem. Chem. Phys*. **1999**, *1*, 5241.
(26) Torimoto, Y.; Harano, A.; Suda, T.; Sadakata, M. *Jpn. J. Appl. Phys.* **1997**, *36*, L238.
(27) Torimoto, Y.; Nishioka, M.; Sadakata, M. *J. Catal.* In press.
(28) Fowler, R. H.; Nordheim, L. *Proc. R. Soc. London, Ser. A* **1928**, *119*, 173.
(29) Zhu, W.; Kochauski, G. P.; Jin, S. *Science (Washington, D.C.)* **1998**, *282*, 1471.
(30) Geis, M.; Efremow, N. N.; Krohn, K. E.; Twichell, J. C.; Lyszczarz, T. M.; Kalish, R.; Greer, J. A.; Tabat, M. D. *Nature (London)* **1998**, *393*, 431.
(31) Somorjai, G. A. *Introduction to Surface Chemistry and Catalysis*; Wiley & Sons: New York, 1994; p 381.
(32) Jackschath, C.; Rabin, I.; Schulze, W. *Ber. Bunsen-Ges. Phys. Chem*. **1992**, *96*, 1200.
(33) Wang, D. Y.; Nowick, A. S. *J. Electrochem. Soc*. **1979**, *126*, 1155.
(34) Wang, D. Y.; Nowick, A. S. *J. Electrochem. Soc*. **1979**, *126*, 1166.
(35) Wang, D. Y.; Nowick, A. S. *J. Electrochem. Soc*. **1981**, *128*, 55.
(36) Smirnor, B. M. *Negative Ions*; McGraw-Hill: New York, 1982.
(37) Hakkinen, H.; Landman, U. *J. Am. Chem. Soc*. **2001**, *123*, 9704.
(38) Saliba, N.; Parker, D. H.; Koel, B. E. *Surf. Sci*. **1998**, *410*, 270.
(39) Ishikawa, J. *J. Surf. Coat. Technol*. **1996**, *65*, 64.
(40) Ishikawa, J.; Takeiri, Y.; Tagaki, T. J. *Rev. Sci. Instrum*. **1993**, *57*, 1512.
(41) Fueno, H.; Ikuta, S. *Chem. Phys. Lett*. **1993**, *204*, 320.